Advances in Coastal Modeling
edited by C. Lakhan

Chapter 15

Merging Scales in Models of Water Circulation: Perspectives from the Great Barrier Reef

Eric Wolanski [a], Richard Brinkman [a], Simon Spagnol [a], Felicity McAllister [a], Craig Steinberg [a], William Skirving [a] and Eric Deleersnijder [b]

[a] Australian Institute of Marine Science, PMB No. 3, Townsville MC, Queensland 4810 Australia
[b] Institut d'Astronomie et de Geophysique G. Lemaitre, Universite Catholique de Louvain, 2 Chemin du Cyclotron, B-1348 Louvain-La-Neuve, Belgium

1. INTRODUCTION

Several challenges exist in modeling ocean circulation across a range of spatial and temporal scales. By focusing on the domain of the Great Barrier Reef this chapter emphasizes that a better understanding of large-scale water circulation can be obtained by merging scales to allow for feedbacks between smaller scale and coarser scale models. The Great Barrier Reef (GBR) (Fig. 1a) comprises more than 2800 individual reefs that are spread over a 2600 km length of Australia's north-eastern continental shelf, at the western margin of the Coral Sea. The topography is highly complex, with individual reefs ranging in area from 0.01 to 100 km^2. In some regions the reefs form a ribbon separated by narrow passages (Fig. 1b), and occupy approximately 90% of the along-shelf length, thus providing a significant barrier to the water circulation (Pickard et al., 1977). In other regions the reefs are widely scattered, separated by wide passages and occupy only about 10% of the along-shelf length (Fig. 1c). The continental shelf water depth tends to gently slope to around 100 m at the shelf break. The interaction of this complex topography, the wind, the tides, and the circulation in the adjoining Coral Sea all serve to strongly influence the circulation on the GBR shelf (Wolanski, 1994). This circulation plays a crucial role in a number of important biological processes, including the: (a) flushing of Great Barrier Reef waters by Coral Sea waters, (b) connectivity of reef populations as a result of the transport of water-borne larvae between reefs, (c) transport of nutrients and pollutants by water currents, (d) retention of fish larvae behind salient topographic features, (e) reef-induced upwelling controlling plankton dynamics, coral health, the location of meadows of the alga *Halimeda*, and (f) role of reef-induced temperature mixing in inhibiting coral bleaching (Andrews, 1983; Andrews and Furnas, 1986; Wolanski and Hamner, 1988; Wolanski et al., 1988; Oliver et al., 1992; Hughes, 1993; Sammarco and Heron, 1994; Wolanski, 1994; Wolanski et al., 1997; Hoegh-Guldberg, 1999; Skirving and Guinotte, 2001; Wolanski, 2001; Brinkman et al., 2002).

With operational processes occurring over a wide range of scales in both space and time, ranging from meters to hundreds of kilometers, and from minutes to years, it is not possible to model the whole GBR domain, including the adjoining western Coral Sea, using a fine-grid, three-dimensional (3-D) model at present. Instead, different two-dimensional (2-D) and 3-D models are used at different scales to study different processes. The merging of these scales and processes remains an art, and examples of such merging will be shown in this chapter. This chapter begins with a description of the technique chosen to include the effect of the oceanic circulation in a 2-D model of the large-scale circulation on the continental shelf. This circulation, however, is found to be modulated at an intermediate spatial scale by the interaction of the tidal circulation with individual reefs, and this process is modeled by merging large-scale and reef-scale 2-D circulation models. To further investigate the

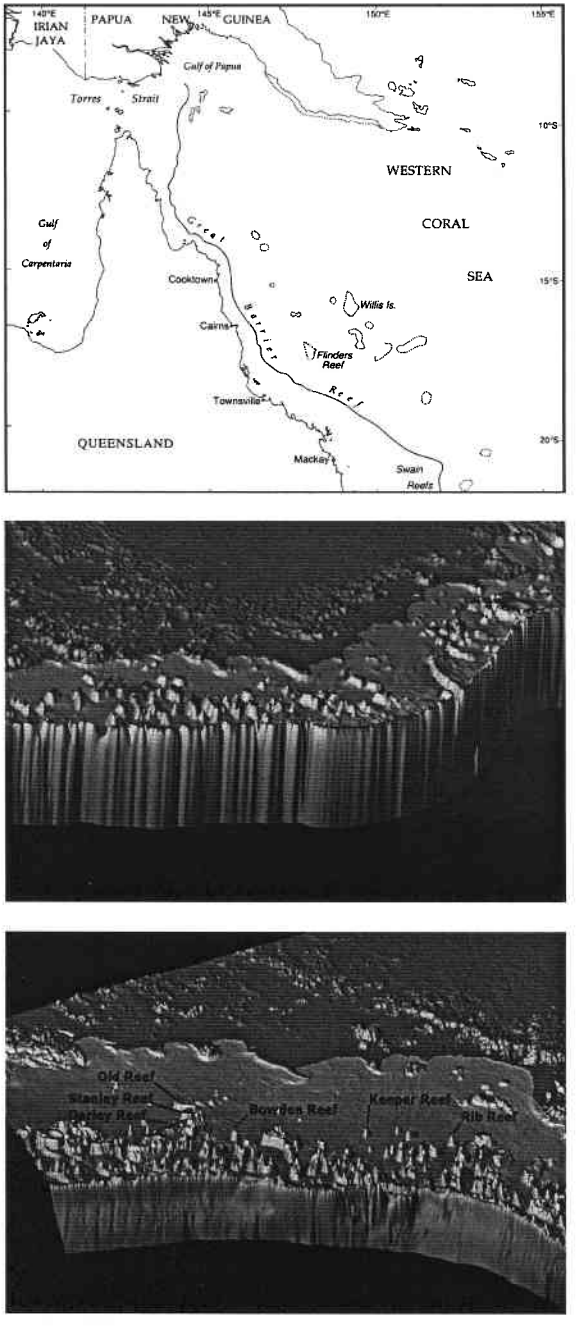

Figure 1. (a) General location map of the Great Barrier Reef. Three-dimensional rendering of the topography of the Great Barrier Reef (b) in the northern region where reefs form a ribbon-like structure, and (c) in the central region where reefs are more widely scattered. Note that the vertical scale of bathymetry has been exaggerated.

circulation around reefs, the reef-scale circulation (the island wake) around one reef in well-mixed coastal waters is studied using 2-D and 3-D models. It is shown that the horizontal properties of the island wake are well reproduced by 2-D models, and that the three-dimensional processes, including upwelling and downwelling, cannot be reliably captured by 3-D modeling except if subgrid scale processes are parameterized. The tidal jet is another reef-scale process generated by strong tidal flows in a reef passage, and this is also investigated using a 3-D model. Finally, a brief discussion is presented of the use of these models to calculate the vertical profiles of temperature in the waters near reefs.

2. THE INFLUENCE OF THE OCEANIC CIRCULATION ON THE GBR SHELF

The circulation in the Coral Sea acts in union with mesoscale wind events and tidal forcing to control the circulation on the GBR shelf (Church, 1987; Andrews and Clegg, 1989; Wolanski, 1994; Brinkman et al., 2002). In the Coral Sea, a westward flowing jet bifurcates as it approaches the Australian continental margin (Fig. 2). This results in two currents along the edge of the shelf; namely the Coral Sea Coastal Current that flows northward from the bifurcation point, and the East Australian Current that flows southward of the bifurcation point (Andrews and Clegg, 1989; Wolanski, 1994). The East Australian Current has a typical speed of 0.3 m s^{-1} in the upper 200 m of shelf break waters of the central GBR (Church and Boland, 1983); the current is halved at a depth of 100 m (Wolanski, 1994). Long-term studies have not been done on the strength and location of the oceanic jet in the Coral Sea creating this circulation. However, data from long-term moorings on the GBR outer continental shelf are available. These data suggest that the location of the bifurcation point varies seasonally and inter-annually.

The Coral Sea circulation is thus expected to generate both a cross-shelf and a longshore regional sea level gradient on the GBR shelf (Middleton, 1987). To the south of the bifurcation point the

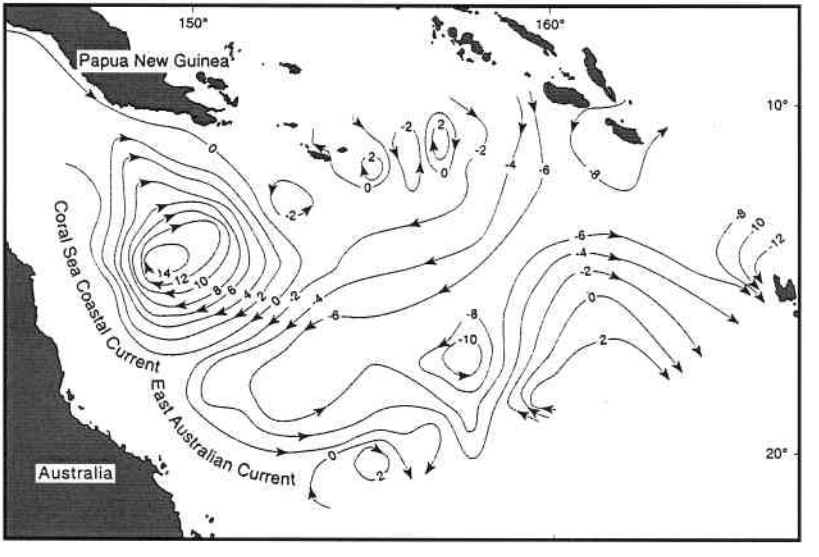

Figure 2. Contours of volume transport (in Sv) for the top 1000 m at 2.4 Sv intervals for the Western Coral Sea. Adapted from Andrews and Clegg (1989).

longshore surface slope induces a southward net flow on the GBR shelf, which displays strong inter-annual and seasonal fluctuations due to variability in the circulation in the Coral Sea (Wolanski, 1994). Similarly, north of the bifurcation point a net northward longshore flow exists on the GBR shelf (Brinkman et al., 2002). Analysis of long-term current meter records from moorings at various locations along the length of the central GBR region reveals the magnitude of these persistent, but variable net currents. The observed change of direction of the longshore net current between southern and northern mooring locations indicated that an oceanic inflow had occurred between these mooring sites, at latitudes 14.7°S and 16.75°S respectively. This cross-shelf component of the circulation is biologically important as it controls the flushing of the GBR by the Coral Sea, and hence the residence time of water on the GBR shelf.

3. MODEL PARAMETERIZATION

To model the influence of regional sea surface gradients on the circulation on the GBR shelf, a 2-D model was considered appropriate as the shelf waters are generally well-mixed throughout the year and flow is primarily horizontal (Wolanski, 1994). Regional sea surface gradients were parameterized in the model by defining the instantaneous sea surface elevation above mean sea level, η, as being composed of a mean elevation, $\bar{\eta}$, plus a time varying fluctuation, η', about this mean

$$\eta = \bar{\eta} + \eta' \tag{1}$$

Decomposition of the sea surface elevation into mean and fluctuating components allowed η' to be used as the prognostic variable for sea surface elevation, and presented an opportunity for regional sea level gradients, $\partial\bar{\eta}/\partial x$ and $\partial\bar{\eta}/\partial y$, to be additional model forcing parameters prescribed as independent values at each computational point and not just at the open boundaries.

The model domain covered a 500 km stretch of the continental shelf from Bowen, in the south, to Lizard Island in the north, and extended into the western Coral Sea. The computational grid for the model was a mesh of 2.0 x 2.0 km spatial resolution, and total grid dimensions of 343 x 138 computational points. The mesh size was sufficiently small to resolve the topographical influence of the reefs in the study region. Localized, reef-induced three-dimensional circulation features known to occur at much smaller scales ($\approx$ 10–500 m) (see Wolanski and Hamner, 1988; Deleersnijder et al., 1992; Wolanski et al., 1996) were not resolved by this model.

The open model boundaries to the northwest, northeast and southeast were forced by sea surface elevation, η, from long-term tide gauge moorings. At the closed coastal boundary and at island and emergent reef boundaries in the interior of the domain, zero transport perpendicular to the boundary was specified. Data from a weather station within the model domain prescribed the wind forcing. Regional sea level gradients, however, were not known explicitly. Such gradients are difficult to measure due to their large spatial and temporal variability. Instead, these slopes were inferred from the analysis of the observed low-frequency longshore currents, which identified a northward net flow in the northern region of the model domain, and a southward net flow in the southern region of the model domain. The region with zero sea surface gradients on the shelf represented the area immediately inshore of the bifurcation point on the continental slope, and defined a zone of inflow from the Coral Sea. Forcing by regional sea surface gradients was only applied on the shelf where bottom friction maintains numerical stability. The absolute values of the gradients were determined by adjusting the magnitude, extent and location of the regional gradients until there was adequate agreement between predicted and observed low frequency currents at the mooring sites.

3.1. Model Execution and Results

The model was run for a 100-day period coincident with the long-term current observations. With the inclusion of the regional sea surface gradient parameterization, computed low frequency longshore currents at the mooring sites compared well with observations (see Fig. 3). The predicted net circulation (Fig. 4a) shows an inflow from the Coral Sea, the Coral Sea Coastal Current, and the East Australian Current. In the absence of the regional slope parameterization in the model, the observed southward flow in the southern region was significantly underpredicted (Fig. 3), and the computed synoptic distribution of the net current averaged over the 100-day run shows an unrealistic, northward flow over the entire shelf (Fig. 4b).

The topographical influence on the inflow onto the GBR is clearly evident in the spatial distribution of the transport across the shelf edge. The largest inflow, representing more than 50% of the total estimated volume, occurred in a region where the density of coral reefs on the outer shelf is sparse, and thus there is little topographical impediment to oceanic inflow. The predicted volume transport from the Coral Sea into the central region of the GBR represented by the model was estimated to be ~ 0.58 Sv. When regional forcing was neglected, the predicted cross-shelf transport was negligible (~ 0.008 Sv).

The oceanic inflow onto the central GBR and its spatial variability predicted by the model with parameterization of regional sea surface gradients is confirmed by a satellite image of the chlorophyll concentration in this region at 01:43:51, July 14, 2000 GTM (Fig. 5). In the northern region of the central GBR, north of approximately 16°S, inflows are limited to very distinct channels between the otherwise highly dense reef matrices. South of 16°S, where the spatial density of the reef matrix decreases, oceanic inflows become more spatially frequent, with a major zone of inflow evident between Rib Reef and Bowden Reef. Further south from Bowden Reef there is minimal inflow across the outer shelf inflow due to the presence of the dense reef matrix on the outer shelf. On the mid-shelf, however, oceanic water originating from inflows further north appears as a dark plume with distinct frontal features. This image also suggest that there can exist quite distinct cross-shelf fronts between coastal waters and waters of oceanic origin. A subsequent image collected at 02:06:10, July 15, 2000 GMT (not shown) revealed that the oceanic/coastal-water front south of Bowden Reef had

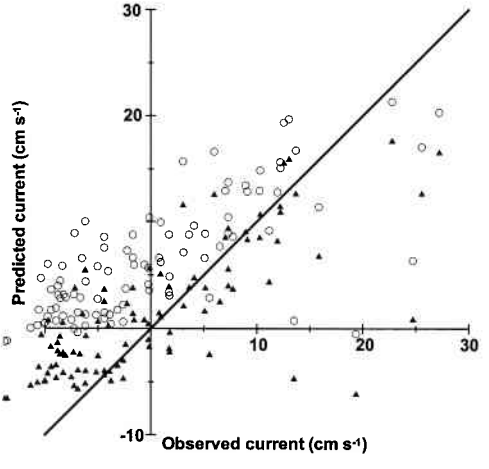

Figure 3. Scatter plots of observed and predicted daily mean currents at the Cape Upstart mooring site for (o) no forcing and (▲) forcing by regional sea surface gradients.

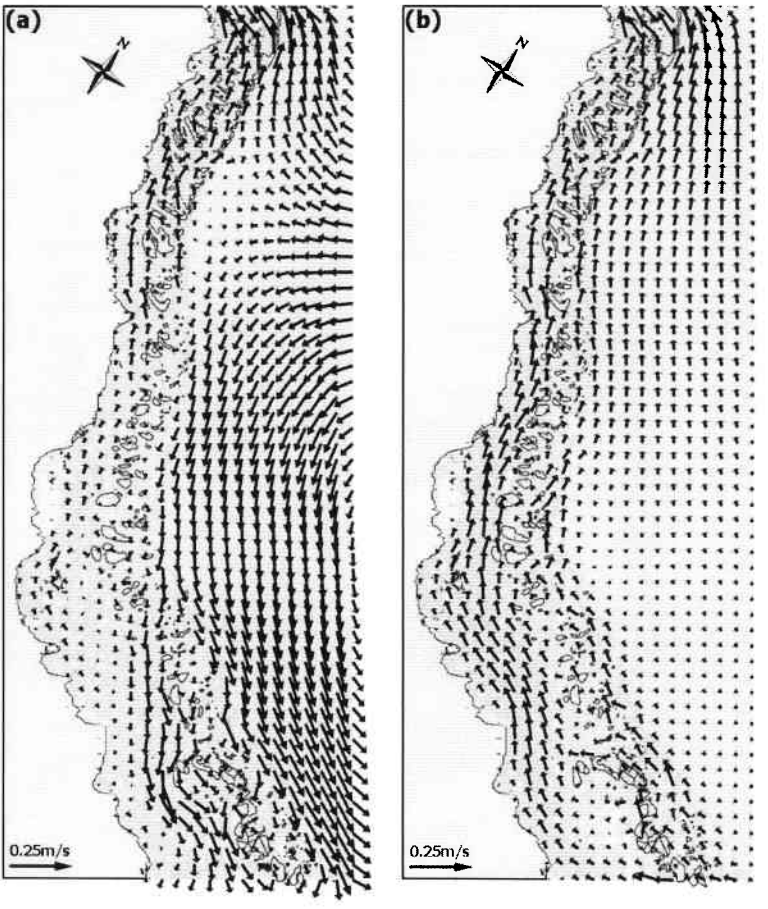

Figure 4. Synoptic views of mean currents over the 100 days of the model run in the austral winter of 1981 under the influence of wind and tides, and (a) forcing by regional sea surface gradients, and (b) no forcing by regional sea surface gradients.

penetrated approximately 16.5 km further southwards with an average speed of approximately 0.18 m s^{-1}.

4. FLOW AROUND OBSTACLES: AN ARCHIPELAGO

The southward flowing East Australian Current meets a system of reefs including Old, Stanley and Darley Reefs (Fig. 1c). This matrix includes a few narrow passages, typically 0.5–2 km in width. Data from current meter moorings have shown that the East Australian Current flows through such passages at neap tides (tidal range $\approx$ 2 m) and water in the reef matrix is rapidly flushed. However, at spring tides (tidal range $\approx$ 4 m), the East Australian Current is deflected sideways around the reef matrix and does not flow through the reef passages. In such cases the water inside the reef matrix is essentially trapped (Wolanski and Spagnol, 2000; Spagnol et al., 2001).

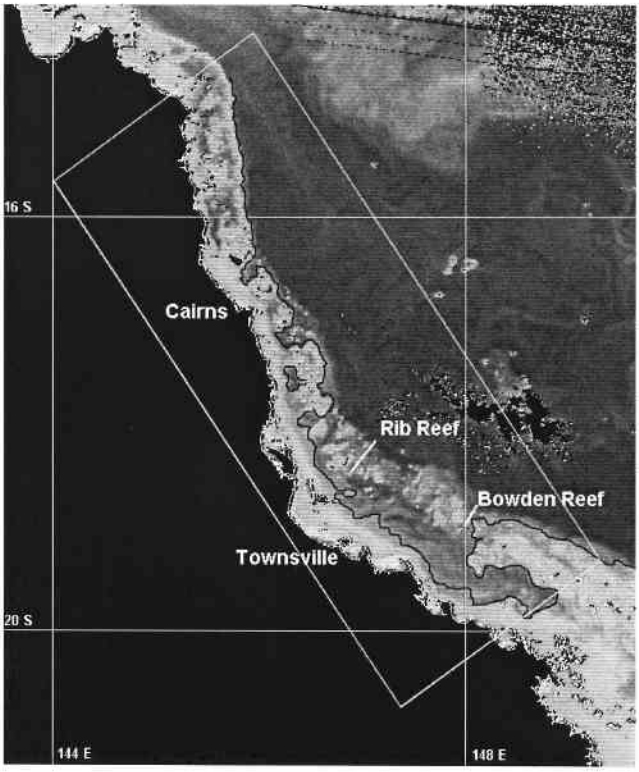

Figure 5. SeaWiFS satellite image of chlorophyll a concentrations in the central Great Barrier Reef, at 01:43:51, July 14, 2000 GMT. Darker areas indicate water of oceanic origin with low chlorophyll concentrations. Lighter areas are either chlorophyll rich shelf waters or turbid coastal water. The solid black contour line delineates waters of coastal and oceanic origin. Black areas are land or cloud. The model domain of the present study is indicated by the enclosed rectangle. The image was received and processed by the Australian Institute of Marine Science, courtesy of Orbimage. Adapted from Brinkman et al. (2002).

To model this process, the general circulation model including the regional slope parameterization (see Section 3) was used to force a 2-D model with a horizontal scale of 500 m. The model was run separately for neap and spring tides. At neap tides, tidal and mean currents are of similar magnitude and the East Australian Current is able to filter through the reef passages (Fig. 6). At spring tides the water entering the reef passage originates from a narrow band around the reef. Outside of this band, the water is deflected around the reef and the reef matrix is thus impermeable to the bulk of the water upstream.

This deflection is made obvious by the evolution of a plume of passive tracers released upstream from this reef matrix. As shown in Fig. 7, at neap tides a fraction of the plume spreads and diffuses through the reef matrix. At spring tides, however, the whole plume is deflected around the reef matrix. This has important biological implications in that the connectivity between reefs for water-borne larvae (including coral and fish) is quite different at spring and neap tides.

The reason for this process appears to be the high dissipation of energy and the resulting high tidal friction at spring tides as a result of the flow around and through the reef matrix. Satellite imagery (Fig. 8) shows island wakes and tidal jets in the lee of reefs, and Sections 5 and 6 describe models of

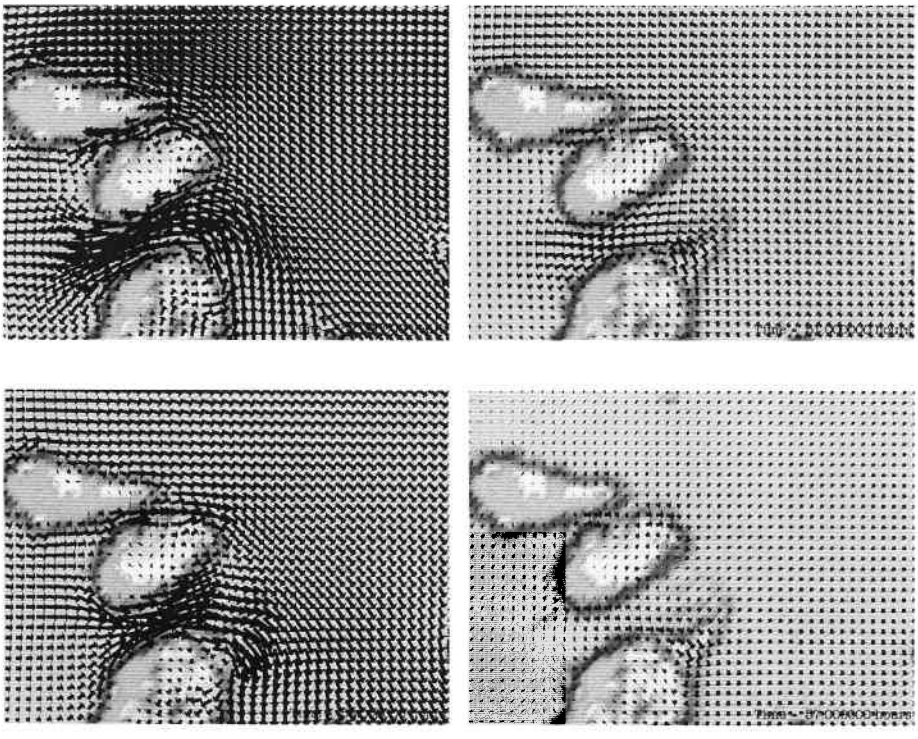

Figure 6. Predicted synoptic distribution of the velocity field on a windless day around Old, Stanley and Darley Reefs (see a location map in Fig. 1c) at (top) peak flood tide and (bottom) peak ebb tide for (left) spring tides and (right) neap tides, for the same regional sea level gradient forced by the Coral Sea. North is to the right. Adapted from Spagnol et al. (2001).

these phenomena. The dissipation of energy in forming an island wake is found to vary nonlinearly with the square of the water current speed. This suggests that four times more energy is dissipated in driving the East Australian Current through the reef matrix at spring tides, than at neap tides.

5. FLOW AROUND OBSTACLES: ONE REEF

The flow around a single reef appears two-dimensional because a reef is typically a few kilometers in size while water depth is typically 20–50 m. Little was known of the dynamics of such flows until a detailed field study was carried out at Rattray Island situated 20°S (Wolanski, 1994). This island is 1.5 km long and 300 m wide and lies in well-mixed coastal waters 20 to 30 m deep. Its long axis is oriented at about 60° to the direction of the dominant semidiurnal flood-tidal current. Flood-tidal currents generate an island wake in the lee of the island. This wake, measured using 26 moored current meters (Fig. 9a), takes the shape of a well-organized eddy growing in time to up to twice the island's width. This wake differs from that expected from laboratory experiments of flows around obstacles because the apparent Reynolds number (assuming a horizontal eddy viscosity of 1.5 $m^2\ s^{-1}$) (see Okubo, 1974; Fischer et al., 1979) is about 400, which in laboratory experiments

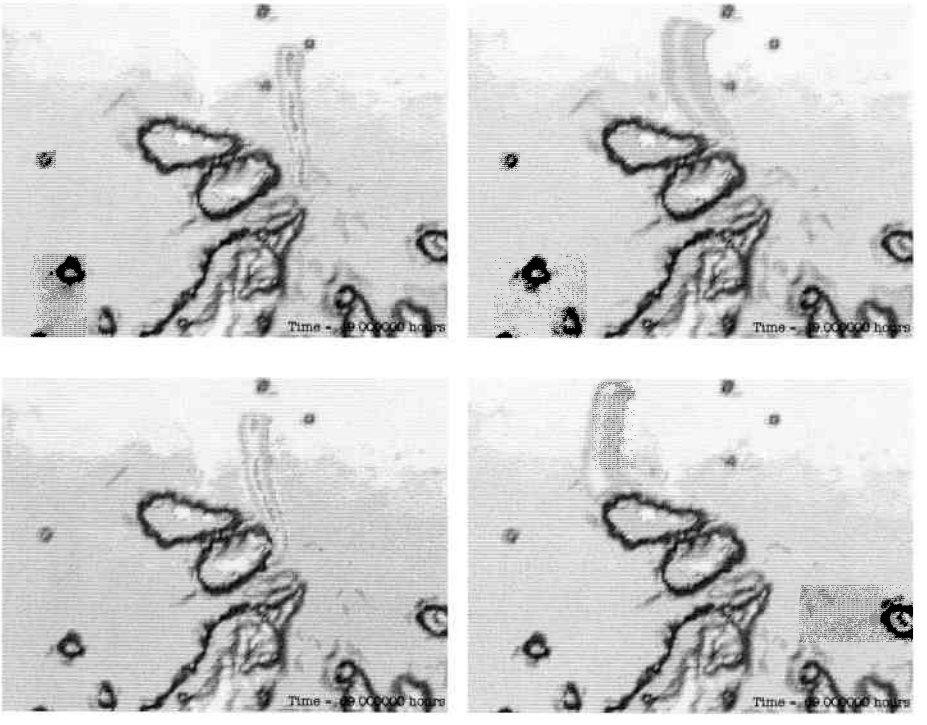

Figure 7. Predicted synoptic distribution of a passive tracer released upstream from Old, Stanley and Darley Reefs under no wind conditions, for (left) neap tides and (right) spring tides, at (top) time=0 and (bottom) time=20 hours, for the same regional sea level gradient forced by the Coral Sea. North is to the right. Note that part of the plume is advected through the reef passages at neap tides only, and that the whole plume is deflected sideways at spring tides. Adapted from Spagnol et al. (2001).

implies a long turbulent wake. In laboratory experiments a distinct eddy of a shape similar to that at Rattray Island forms for a Reynolds number of about 1–20.

A further difference between the eddy at Rattray Island and that in laboratory experiments is found in the different values of the ratio u/U, where u is the maximum velocity in the eddy, and U is the maximum velocity of the prevailing mean flow. At Rattray Island, $u/U = 0.75$, whereas in laboratory experiments $u/U \approx 0.01$. This observation suggests that the aspect ratio W/H is important, where W is the width of the island (the obstacle) and H is the depth. At Rattray Island, $W/H \gg 1$, while in laboratory experiments $W/H \ll 1$. This finding suggests that bottom friction is important for flows around coral reefs.

Depth-averaged, finite-difference 2-D models are able to reproduce quite accurately the horizontal velocity field (Fig. 9b). Discrete vortex models are also quite successful (not shown, see Furukawa and Wolanski, 1998).

Further, visual observations reveal that the eddies are also strongly three-dimensional because bottom mud is brought to the surface in the eddy center within one hour of eddy formation in water depth of 25 m, implying a vertical upward velocity of 5.5 mm/s. Visual observations also reveal that such eddies trap floating matter (for example, coral eggs) along their outer boundaries, implying a downward velocity near the outer edges of the eddy (Wolanski, 1994). Wolanski et al. (1996) carried out laboratory experiments on island wakes where the aspect ratio $W/H \ll 1$. They found a

Figure 8. Satellite image of the Great Barrier Reef off the Whitsunday Islands (20°S). Note the vortices are streaming between narrow reef passages. Image courtesy of NASA/GSFC/LaRC/JPL MISR Team.

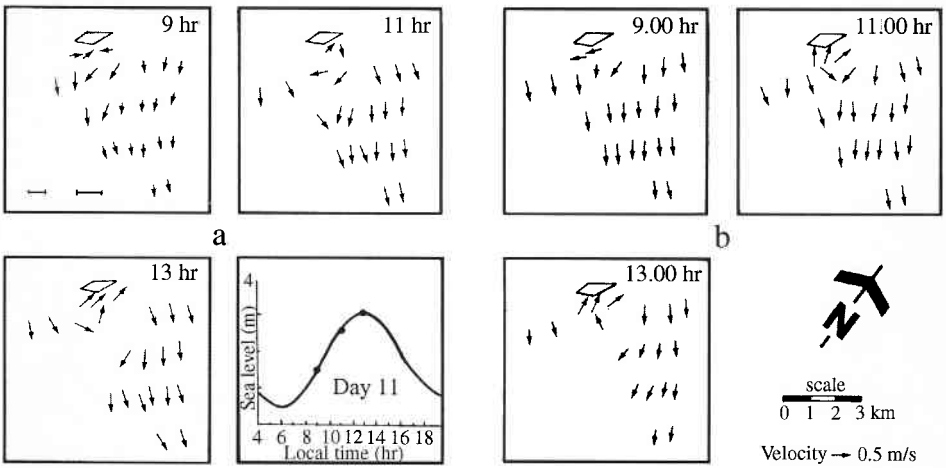

Figure 9. (a) Observed distribution of currents around Rattray Island at flood tide, at current meter mooring sites. (b) Predicted distribution at the same sites, from a depth-averaged 2-D model. Adapted from Wolanski (1994).

strong upwelling in the eddy center and an even stronger downwelling along the edges of the eddy. To calculate this three-dimensional circulation and to compare the ability of various 3-D models to reproduce such flows, five different 3-D models were used to model the island wake at Rattray Island. These models used the same bathymetry, horizontal grid size (200 m) and open boundary forcing (currents on the northern open boundary and tidal elevation on the southern open boundary) taken directly from the field data on currents and tides. The 3-D models were the Princeton Ocean Model (POM) (Blumberg and Mellor, 1987), the AIMS-GHER model (Deleersnijder et al., 1992),

Table 1
Summary of five 3-D model simulations and results for the wake behind Rattray Island.

Model	Vertical Coordinate	L/L_0	u/U
POM	α	0.5	0.5
AIMS-GHER	α	0.6	0.6
MECCA	α	No eddy	No eddy
HAMSOM	z	0.2	0.2
MECO (a)	z	No eddy	No eddy
MECO (b)	z	0.8	0.4

L = predicted maximum eddy size. L_0 = observed maximum eddy size. u = predicted maximum velocity in the eddy. U = observed maximum velocity in the field. In the field, $u/U = 0.75$. Results from the first four models are adapted from Galloway et al. (1996). (a) Result when the model and prototype eddies are compared at the same time; (b) result when the model is allowed to run an extra hour.

the MECCA model (Hess, 1989), the HAMSON model (Stronach et al., 1993) and the MECO model (Walker and Waring, 1998).

The ability of the models to reproduce the observations was estimated by comparing the maximum predicted (L) and measured (L_0) eddy size, and the maximum predicted (u) and measured (U) velocity in the eddy. As summarized in Table 1, it is apparent that while those 3-D models differ in their ability to reproduce the observations, they all significantly under-estimate by at least 40% the horizontal eddy size as well as the circulation in the eddy. Since the 2-D models do not appear to suffer from this problem (Fig. 9), this observation suggests that the parameterization of processes in 3-D models near a salient bathymetry may need improvements. Indeed, while the models predicted an upwelling in the eddy center, the upward velocity was significantly underpredicted (≈ 0.5 mm/s as opposed to 5 mm/s in the field). Further, none of the models predicted a downwelling along the outer edges of the eddy.

To improve the ability of 3-D models to reproduce island wakes, Wolanski et al. (1996) explicitly parameterized, in the AIMS-GHER 3-D model, the intense turbulence present in the free shear layer downstream of the separation points at the tips of the island. This free shear layer was too thin to be resolved by the 200 m horizontal grid. This parameterization locally enhanced the value of the vertical eddy diffusivity in the subgrid scale free shear layer. The results were encouraging, in that the AIMS-GHER 3-D model predicted both downwelling along the eddy edges and upwelling at the eddy center (Fig. 10), although their magnitudes were still underpredicted by 50%. However, this parameterization of the free shear layer resulted in a more realistic representation of the horizontal properties of the eddy. Indeed, with this parameterization, $L/L_0 \approx 0.9$, as opposed to ≈ 0.6 without this parameterization (see Table 1). Similarly, $u/U \approx 0.9$, as opposed to ≈ 0.6, with and without this parameterization, respectively. The reason appears to be that the high eddy viscosity in the free shear layer effectively prevents eddy water, containing vorticity generated at the separation point, from escaping the eddy at the surface and vorticity-free oceanic water from entering the eddy near the bottom. Since vorticity is retained, the eddy spins up faster.

Two-dimensional, depth-averaged models do not suffer from the problem of the vertical shear of velocity advecting vorticity away since they do not allow shear flows with opposite directions at the surface and at the bottom, therefore such models are better able than 3-D models (without free shear layer parameterization) to reproduce the eddy.

Three-dimensional models underpredict the upwelling in island wakes, by 90% without free-shear layer parameterization, and by 50% with this parameterization. It is, however, these vertical motions which are of most interest to biologists. It remains unclear how to improve the models to make them perform more realistically. At present, the vertical eddy diffusion coefficient is calculated from

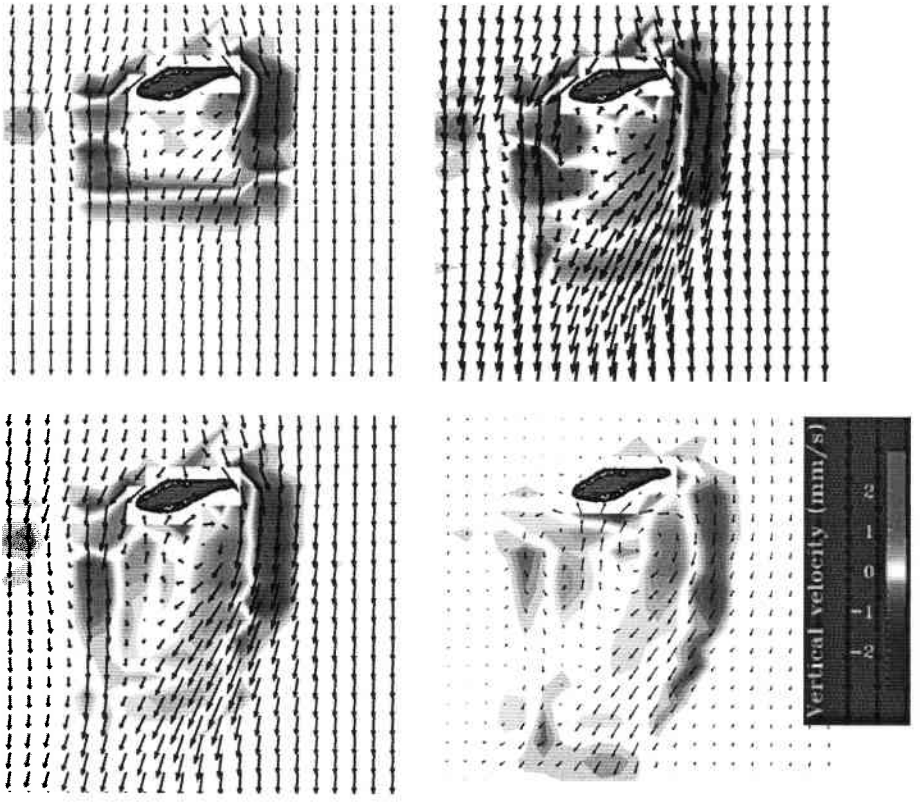

Figure 10. Clockwise starting from top left, synoptic distribution at two-hourly intervals of the predicted 3-D circulation around Rattray Island at flood tide, using the AIMS-GHER model when the free shear layer was explicitly parameterized. The horizontal velocity field at mid-depth is shown by arrows (maximum current ≈ 0.7 m/s, the vertical distribution by shading (a positive value = upwelling, negative value = downwelling; the maximum value ≈ 2 mm/s).

classical, open-channel flow theory. Laboratory experiments where the aspect ratio was conserved (Wolanski et al., 1996) tentatively suggest that bottom-induced turbulence may be reduced in island wakes. This suggests that models could possibly be improved by modifying the parameterization of the vertical eddy viscosity in island wakes. However, this has not been attempted yet, and the models still underperform, because supporting field data are not available. Modeling island wakes remains a rich area of research.

6. FLOW AROUND OBSTACLES: TWO REEFS

Tidal flow through reef passages generates unsteady tidal jets. These systems comprise an inertial jet entraining surrounding water into the jet, and an eddy pair at the leading edge (Wolanski, 1994). In aerial and satellite pictures (Fig. 8) these jets superficially look like mushroom shaped circulation patterns. Like island wakes, these systems also appear two-dimensional because they have an aspect ratio $W/H \gg 1$. As a result, the large-scale dynamics of these systems are successfully reproduced

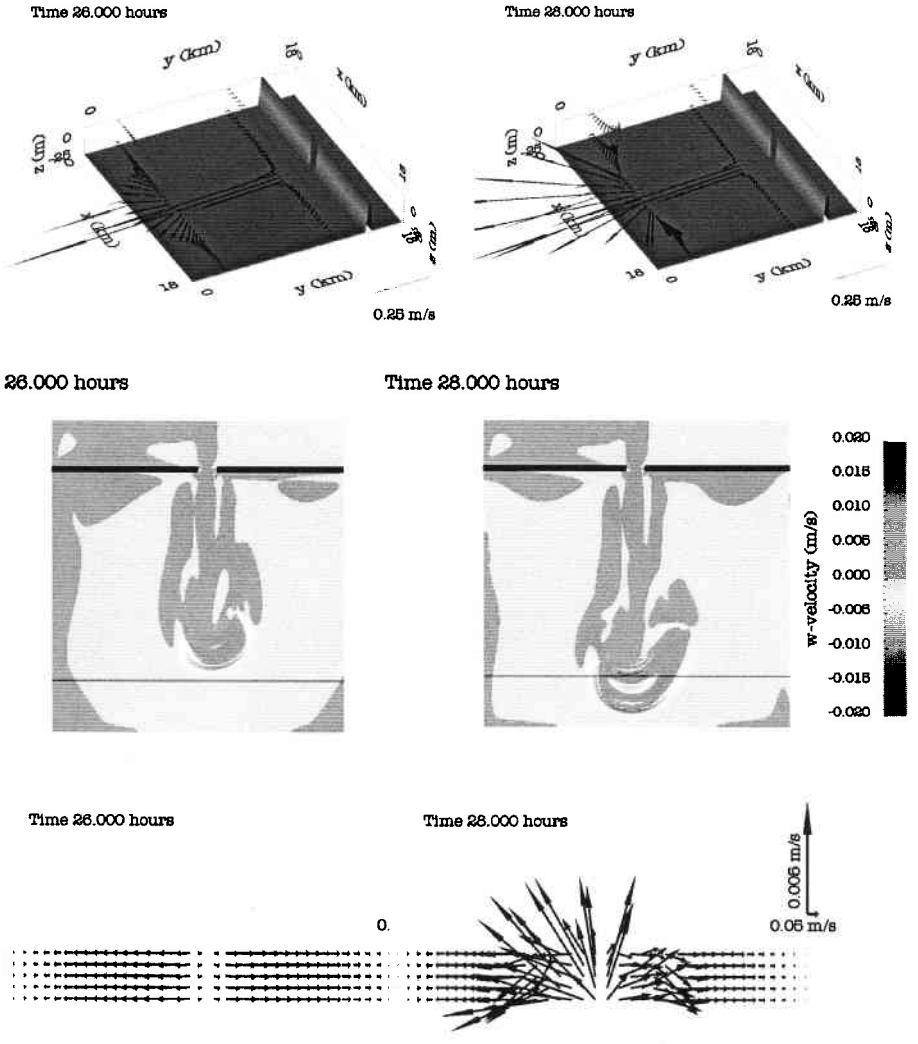

Figure 11. Two synoptic distributions, two hours apart, of the predicted, 3-D velocity field in a tidal jet emanating from the reef passage shown in the top figure in a 3-D rendering of the bathymetry. The top figures show in 3-D at two cross-sections the horizontal velocity field near the surface, and near the bottom. The middle figures show the vertical velocity distribution at mid-depth; the scale is shown by the bar on the far right. The bottom figures show the velocity field in a cross-section shown as the thin line in the middle figure. Thus, the figure on the left shows the velocity field upstream of the incoming tidal jet, and the figure on the right shows the velocity field in the upwelling core of the eddy pair at the leading edge of the tidal jet. In the bottom figures, the vertical velocity scale is much larger than the horizontal one.

by two-dimensional, depth-averaged models (Wolanski et al., 1988). However, the key biological process that oceanographers must understand for tidal jets remains the vertical motions which 2-D models do not resolve. Upwelling motions are strong (several mm/s to cm/s) and appear localized at two sites, namely the free-shear layer of the tidal jet and the center of the eddy, as revealed by

visual observations that these jets are turbid, and by CTD and laboratory studies (Onishi, 1984; van Senden and Imberger, 1990; Wolanski, 1994). To attempt to reproduce such flows, the AIMS-GHER 3-D model was used to model the tidal jet resulting from a tidal current peaking at 1 m s^{-1} through a 1 km wide channel facing a shelf sea 25 m deep. The model domain, shown in Fig. 11, was 18 x 18 km wide and the horizontal grid size was 100 m. The model predicted the formation of an unsteady eddy pair tidal jet system (Fig. 11). The jet entrained surrounding oceanic water and grew in width with increasing distance from the reef passage. At its leading edge a vortex pair was generated. Probably because of bottom friction, the jet tended to slide over the oceanic water and generated two weak vortices upstream of the jet and on either side of the jet axis, with a downwelling peaking at a few mm/s. Within the eddy pair, a very strong upwelling was predicted, peaking at 15 mm/s. This upwelled water would then reach the surface in only half an hour, suggesting that upwelled nutrients may quickly become available to plankton. The model predicts that some of this water downwells (sinks) on the fringes of the eddy and that the rest of the water spreads radially away. Interestingly, the model predicts that within the tidal jet itself there is a weak downwelling that will help to trap on the bottom nutrient-rich, cold water upwelled by the Bernoulli effect on the oceanic side of a reef passage. This nutrient-rich water then would become available to *Halimeda* algae on the bottom. Because of the important biological implications of such motions, field studies are needed.

7. TEMPERATURE DISTRIBUTION

The preceding sections have demonstrated that the complex three-dimensional circulation around coral reefs controls vertical and horizontal mixing and advection. Reef-induced mixing thus controls the horizontal and vertical distribution of temperature throughout the water column, as cooler sub-surface water is upwelled to the surface where it mixes with heated surface water. The importance of this key process was highlighted by the 1998 coral bleaching event. Bleaching means that corals (both hard and soft), as well as giant clams and some other animals like sponges, lose their symbiotic algae *zooxanthellae* and/or the pigments of those algae, such that the coral appears pale to stark white (Yonge and Nicholls, 1931). The algae are expelled when put under stress due to heat or intense solar radiation. The threshold temperature for bleaching may be as little as 1–2°C above the mean monthly summer values (Berkelmans and Willis, 1999). Frequently many corals recover from bleaching, but death may result if the stress is extreme or prolonged (Wilkinson, 2000). The coral bleaching of 1998 was the most geographically widespread ever recorded, and probably the most severe in recorded history. On the GBR mass bleaching occurred in the summer of 1998 during a period of neap tides, low winds and cloud-free skies, conditions optimal for coral bleaching (Skirving and Guinotte, 2001).

Sea surface temperatures sensed from NOAA AVHRR imagery provide evidence for enhanced mixing around reefs. Sea surface temperature was colder within two reef matrices, the Pompey and Swain systems (Fig. 12), and coral bleaching was correspondingly lesser in these regions during the 1998 bleaching event. The three-dimensional baroclinic model MECO (Walker and Waring, 1998) is being used to examine these processes. The solar heating of the water column was modeled for Keeper Reef located in the central GBR (Fig. 1c). The model was forced by short wave radiation data observed at the reef, and data from two temperature loggers deployed at different depths on the reef were used to initialize and verify the development of temperature stratification. The initial observed temperature profile on the 24th of January 1998 (Fig. 13) is well-mixed to approximately 28.3°C. Two weeks later on the 6th of February 1998, at the time of the 1998 bleaching event, the observed profile had developed a stratified structure, with a temperature of 30.75°C at 2 m below the surface, decreasing to 29.2°C at a 10 m depth. The model was run for this 2-week period prior

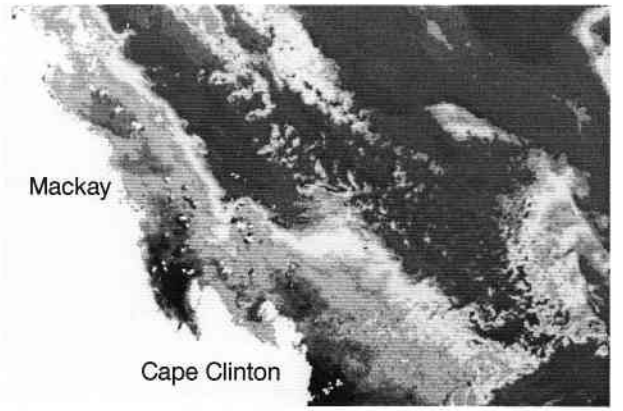

Figure 12. Sea Surface Temperature (SST) image of the Southern GBR from NASA AVHRR satellite during the 1998 coral bleaching event. Offshore between Mackay (21°S) and Cape Clinton (22.5°S) are the Pompey and Swains coral reef systems. These systems are dense reef matrices, their thermal signatures are evident by the patchy nature of the SST, which is colder than surrounding waters. Colder waters were found inshore and within reef matrices.

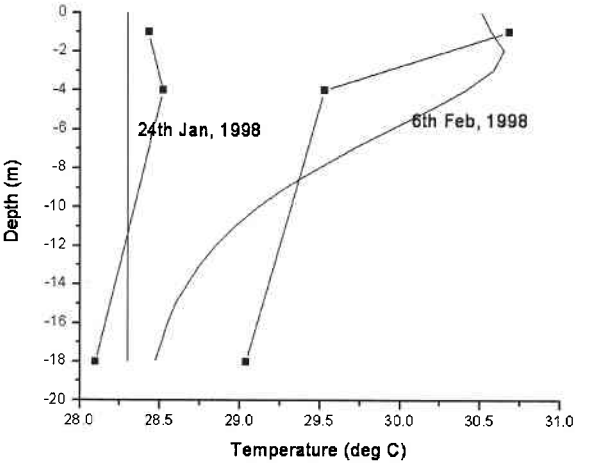

Figure 13. Modeled (smooth lines) and observed (straight lines through filled squares) temperature profile at Keeper Reef (location map in Fig. 1c) during the mass bleaching event in 1998. Temperature data from loggers deployed by the Great Barrier Reef Marine Park Authority.

to the bleaching event, and the predicted final temperature profile compared well with observations (Fig. 13). The predicted profile shows cooler water above the maximum: an effect caused by latent heat loss due to evaporation at the surface. Winds were light and, hence, there occurred little wind-driven mixing in the vertical. The predicted profile is consistent with observations that suggest that approximately three quarters of the total incoming short wave radiation is absorbed within the first 5 m of the ocean (Mann and Lazier, 1996).

It is also important to consider the effect of heating on reef flats. Reef flats are much shallower than the surrounding waters and are generally exposed at low tide. The incoming solar energy is thus partially absorbed in the shallow water and then absorbed, re-radiated and reflected by the reef flat back through the water column. This can significantly increase temperatures and is partly responsible for the elevated temperatures seen in Fig. 13.

Models thus appear effective in predicting the temperature profiles near coral reefs. The predictions are very sensitive to the bathymetry. A key parameter appears to be the density of reef coverage on the shelf—and this varies spatially on the GBR. The two key physical processes are reef-induced turbulence and three-dimensional flows.

It is hoped that models can be used to predict coral bleaching risk maps for the Great Barrier Reef, a tool of increasing need in view of the threat the enhanced Greenhouse effect may pose to the Great Barrier Reef (Hoegh-Guldberg, 1999).

8. DISCUSSIONS

The oceanography of the GBR is made particularly complex by the extraordinary complex bathymetry. The bathymetry interacts with the prevailing circulation at all scales (Fig. 14). As for any other continental shelf, the circulation in the adjoining ocean influences the circulation over the GBR shelf, generating zones of oceanic inflow and longshore currents. In the GBR, however, the obstruction of the flow by the presence of reefs steers and modifies, even at these large scales, the oceanic inflow and the longshore currents. Obstruction by large reefs or a reef matrix steers prevailing currents toward areas of low reef density. This provides the modeler the challenge to merge the large-scale ($\approx$ 1000 km) oceanic circulation with the shelf-scale ($\approx$ 100 km) general distribution of reefs over the shelf. The resulting currents through a reef matrix, and the deflection of the prevailing currents around a reef matrix, are modulated by the tides. This is a process dependent on the bathymetry of passages between reefs, and it presents the modeler yet another challenge to merge the shelf-scale circulation ($\approx$ 100 km) with flow processes in reef passages at horizontal scales of 1.0–0.5 km. While larger scale model grids have spatial resolution (1–2 km) sufficient to adequately describe the majority of the topography, including small islands, reefs and reef passages, these models are not able to accurately reproduce the smaller scale processes that accompany the topography. For example, island wakes and tidal jets alter the friction, which in turn alters the large-scale processes (Fig. 14). The difficulty lies in identifying the small-scale processes that are relevant at larger scales, and then parameterizing these processes in the larger scale models.

The fate of nutrients and larvae is a key biological question that oceanographers must address. This is dependent on details of the currents around individual reefs, which requires the modeler to quantify currents at horizontal scales of the order of 100 m while the prevailing current field varies at horizontal scales of 0.5–2 km. To correctly quantify these three-dimensional processes at horizontal scales of 100 m, the oceanographer, however, has to take into account small-scale processes, such as free-shear layer dynamics, at horizontal scales of meters to tens of meters. All these processes influence the horizontal and vertical distribution of temperature near coral reefs, a key process for the biology as it controls coral survival and health.

A fundamental lesson that has emerged is the need for detailed field studies, occasionally complemented by laboratory studies, of key processes and phenomena. These studies not only provide data for model calibration, they also provide an understanding of key processes that must be incorporated in models, if those models are to successfully reproduce the observed phenomenon. Because of the complex bathymetry, these local physical processes operate at all scales, from subgrid through to scales comparable to the full domain that the modeler attempts to study, while other processes occur at large-scales, such as the oceanic circulation about which field data are not available. Field

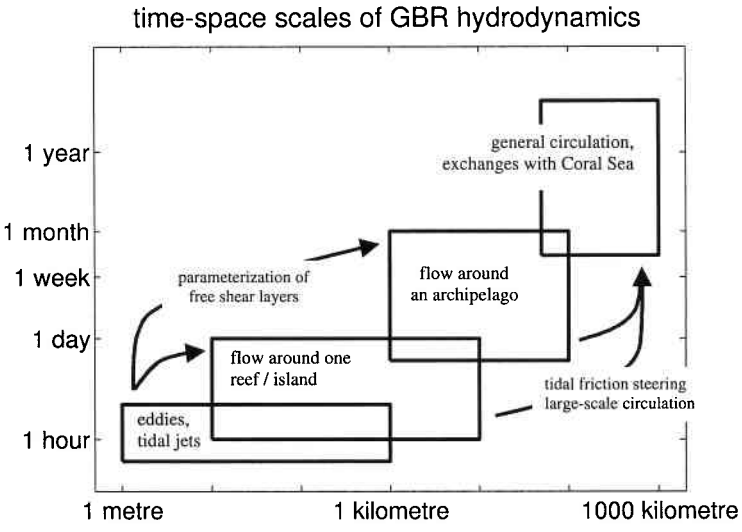

Figure 14. A sketch of the spatial and temporal scales of the dominant processes controlling the circulation in the GBR. The arrows indicate feedback processes.

studies provide an insight on how processes operating at very different spatial and temporal scales interact. They enable the wise modeler to advance their knowledge of the water circulation around the GBR. Modelers focusing on the GBR have become aware that a feedback exists between scales, meaning that small-scale processes have an effect at larger scales. The GBR modeler cannot just perform a one-way "zoom-in" by nesting models of increasingly smaller grid sizes and relying on the coarser models to provide accurate open boundary conditions for smaller scale problems. Instead, the modeler must merge scales judiciously by allowing feedbacks to occur between them (Fig. 14).

Most marine models address a range of time-space scales of motion that is relatively small compared with the complete range of the scales characterizing processes taking place in the sea. For instance, the order of magnitude of the ratio of the largest scale to the smallest one resolved by a model rarely exceeds 100. To broaden the range of space scales simulated numerically, one can have recourse to a variable-resolution grid, which is fine in the regions where it is necessary and is coarser otherwise. Another option is to implement a nested-grid model. However, none of these approaches alleviates the need for appropriate parameterization of subgrid-scale processes. Clearly, the latter depends on the nature of the subgrid-scale phenomena and technical aspects of the modeling of the resolved processes. There are processes that are so peculiar that it is difficult to parameterize them satisfactorily. The broad space-time variability of the GBR provides examples relevant to the present discussion, however, modeling this environment remains nearly an art.

ACKNOWLEDGMENTS

This study was supported by the Australian Institute of Marine Science (AIMS), and IBM-Australia. Eric Deleersnijder is a Research Associate with the National Fund for Scientific Research of Belgium (FNRS).

REFERENCES

Andrews, J.C., 1983. Water masses, nutrient levels and seasonal drift on the Outer Central Queensland Shelf (Great Barrier Reef). Australian Journal of Marine and Freshwater Research, 34: 821–834.

Andrews, J.C., and Clegg, S., 1989. Coral Sea circulation and transport from modal information models. Deep-Sea Research, 36: 957–974.

Andrews, J.C., and Furnas, M.J., 1986. Subsurface intrusions of Coral Sea water into the central Great Barrier Reef—I. Structures and shelf-scale dynamics. Continental Shelf Research, 6: 491–514.

Berkelmans, R., and Willis, B.L., 1999. Seasonal and local spatial patterns in the upper thermal limits of corals on the inshore Central Great Barrier Reef. Coral Reefs, 18: 219–228.

Blumberg, A.F., and Mellor, G.L., 1987. A description of the three-dimensional coastal ocean circulation model. In: Heaps, N. (Editor), Three-Dimensional Coastal Ocean Models, pp. 1–16. Washington, D.C.: American Geophysical Union.

Brinkman, R., Wolanski, E., Deleersnijder, E., McAllister, F., and Skirving, W., 2002. Oceanic inflow from the Coral Sea into the Great Barrier Reef. Estuarine, Coastal and Shelf Science, 54: 655–668.

Church, J.A., 1987. East Australian Current adjacent to the Great Barrier Reef. Australian Journal of Marine and Freshwater Research, 38: 671–683.

Church, J.A., and Boland, F.M., 1983. A permanent under current adjacent to the Great Barrier Reef. Journal of Physical Oceanography, 13: 1747–1749.

Deleersnijder, E., Norro, A., and Wolanski, E., 1992. A three-dimensional model of the water circulation around an island in shallow water. Continental Shelf Research, 12: 891–906.

Fischer, H.B.E., List, E.Y., Koh, R.C.Y., Imberger, J., and Brooks, N.H. , 1979. Mixing in Inland and Coastal Waters. New York: Academic Press, 483p.

Furukawa, K., and Wolanski, E., 1998. Shallow-water frictional effects in island wakes. Estuarine, Coastal and Shelf Science, 46: 599–608.

Galloway, D., Wolanski, E., and King, B., 1996. Modelling eddy formation in coastal waters: a comparison between model capabilities. In: Spaulding, M., and Cheng, R.T. (Editors), Estuarine and Coastal Modelling, pp. 13–25. Reston, VA: American Society Civil Engineers.

Hess, K.W., 1989. MECCA Programs Documentation. NOAA Technical Report NESDIS, 46.

Hoegh-Guldberg, O., 1999. Climate change, coral bleaching and the future of the world's coral reefs. Marine and Freshwater Research, 50: 839–866.

Hughes, R.D., 1993. An Investigation of the Coral Sea with an Ocean General Circulation Model. Ph.D. Thesis. James Cook University of North Queensland, Department of Civil and Systems Engineering, 290p.

Mann, K.H., and Lazier, J.R.N., 1996. Dynamics of Marine Ecosystems, Biological-Physical Interactions in the Oceans. Second Edition. Massachusetts: Blackwell Science, 394p.

Middleton, J.H., 1987. Steady coastal circulation due to oceanic longshore pressure gradients. Journal of Physical Oceanography, 17: 604–612.

Okubo, A., 1974. Effects of shoreline irregularities on streamwise dispersion in estuaries and other embayments. Netherlands Journal of Sea Research, 6: 213–224.

Oliver, J., King, B., Willis, B., Babcock, R., and Wolanski, E., 1992. Dispersal of coral larvae from a coral reef. Comparison between model predictions and observed concentrations. Continental Shelf Research, 12: 873–891.

Onishi, S., 1984. Study of vortex structure in water surface jets by means of remote-sensing. In: Nihoul, J.C.J. (Editor), Remote Sensing of Shelf Seas Hydrodynamics, pp. 107–132. Amsterdam, The Netherlands: Elsevier Science Publishers.

Pickard, G.L., Donguy, J.R., Hennin, C., and Rougerie, F., 1977. A Review of the Physical Oceanography of the Great Barrier Reef and Western Coral Sea. Monograph Series 2. Townsville: Australian Institute of Marine Science, 134p.

Sammarco, P.W., and Heron, M.L. (Editors), 1994. The Bio-Physics of Marine Larval Dispersal, Coastal and Estuarine Studies, Vol. 45. Washington, D.C.: American Geophysical Union, 352p.

Skirving, W., and Guinotte, J., 2001. The sea surface temperature story on the Great Barrier Reef during the Coral bleaching event of 1998. In: Wolanski, E. (Editor), Oceanographic Processes of Coral Reefs: Physical and Biological Links in the Great Barrier Reef, pp. 301–313. Boca Raton, FL: CRC Press.

Spagnol, S., Wolanski, E., and Deleersnijder, E., 2001. Steering by Coral Reef assemblages. In: Wolanski, E. (Editor), Oceanographic Processes of Coral Reefs: Physical and Biological Links in the Great Barrier Reef, pp. 231–236. Boca Raton, FL: CRC Press.

Stronach, J.A., Backhaus, J.O., and Murty, T.S., 1993. An update on the numerical simulation of oceanographic processes in waters between Vancouver Island and the mainland: the GF8 model. Oceanography and Marine Biology Annual Review, 31: 1–86.

van Senden, D., and Imberger, J., 1990. Effects of initial condition and Ekman suction on tidal outflows from inlets. Journal of Geophysical Research, 95: 13,373–12,291.

Walker, S.J., and Waring, J.R., 1998. Model for Estuaries and Coastal Oceans. CSIRO Internal Report No. OMR-118/120, 77p.

Wilkinson, C.R., 2000. Status of Coral Reefs of the World: 2000. Townsville: Australian Institute of Marine Science, 363p.

Wolanski, E., 1994. Physical Oceanographic Processes of the Great Barrier Reef. Boca Raton, FL: CRC Press, 194p.

Wolanski, E. (Editor), 2001. Oceanographic Processes on Coral Reefs: Physical and Biological Links in the Great Barrier Reef. Boca Raton, FL: CRC Press, 356p.

Wolanski, E., Asaeda, T., Tanaka, A., and Deleersnijder, E., 1996. Three-dimensional island wakes in the field, laboratory and numerical models. Continental Shelf Research, 16: 1437–1452.

Wolanski, E., Doherty, P., and Carleton, J., 1997. Directional swimming of fish larvae determines connectivity of fish populations on the Great Barrier Reef. Naturwissenschaften, 84: 262–268.

Wolanski, E., Drew, E., Abel, K., and O'Brien, J., 1988. Tidal jets, nutrient upwelling and their influence on the productivity of the algal *Halimeda* in the Ribbon Reefs, Great Barrier Reef. Estuarine, Coastal and Shelf Science, 26: 169–201.

Wolanski, E., and Hamner, W.M., 1988. Topographically controlled fronts in the ocean and their biological influence. Science, 241: 177–181.

Wolanski, E., and Spagnol, S., 2000. Sticky waters in the Great Barrier Reef. Estuarine, Coastal and Shelf Science, 50: 27–32.

Yonge, C.M., and Nicholls, A.G., 1931. Studies on the physiology of the *zooxanthellae*. Science Report, Great Barrier Reef Expedition (1928–1929), Vol. 1, pp. 135–176.